Hindawi
Complexity
Volume 2019, Article ID 2941835, 14 pages
https://doi.org/10.1155/2019/2941835

Research Article

Enhancing Ikeda Time Delay System by Breaking the Symmetry of Sine Nonlinearity

Xiaojing Gao

School of Computer Science, China University of Geosciences, Building No. 1, North Campus, CUG Lumo Road 388, Wuhan 430074, China

Correspondence should be addressed to Xiaojing Gao; gaoxj@cug.edu.cn

Received 23 August 2019; Accepted 25 November 2019; Published 16 December 2019

Guest Editor: Serdar Çiçek

In the present contribution, an asymmetric central contraction mutation (ACCM) model is proposed to enhance the Ikeda time delay system. The modified Ikeda system model is designed by introducing a superimposed tanh function term into the sine nonlinearity term. Stability and Hopf bifurcation characteristics of the system are analyzed theoretically. Numerical simulations, carried out in terms of bifurcation diagrams, Lyapunov exponents spectrum, phase portraits, and two-parameter (2D) largest Lyapunov exponent diagrams are employed to highlight the complex dynamical behaviors exhibited by the enhanced system. The results indicate that the modified system has rich dynamical behaviors including limit cycle, multiscroll hyperchaos, chaos, and hyperchaos. Moreover, as a major outcome of this paper, considering the fragile chaos phenomenon, the ACCM-Ikeda time delay system has better dynamical complexity and larger connected chaotic parameter spaces (connectedness means that there is no stripe corresponding to nonchaotic dynamics embedded in the chaos regions).

1. Introduction

Chaotic system has many specific properties, such as initial state and parameters sensitivity, unpredictability, and topological mixing [1–3]. Although the equation model of a chaotic system is deterministic, it is impossible to predict its long-term behavior. These meaningful properties make chaotic systems widely studied and applied in many disciplines [4–10]. Specially, with the rapid development of information society chaos, secure communication has already been established to be a good candidate for transmission of confidential message [11–13]. In addition, chaotic systems have important applications in chaos-based random number generation [14] and sensors [15].

In recent years, time delay (TD) systems have become the subject of active research, which stems from the following reasons: (i) the existence of TD in nonlinear systems makes systems more complex. It has been found that communication systems based on low-dimensional chaotic systems (having a single positive LE) are insecure because their dynamics can be easily reconstructed by Takens' embedding theorem [16]. TD chaotic systems modelled by nonlinear delay differential equations (DDEs) exhibit infinite dimensional phase space that cannot be anticipated by a low-dimensional system. As such, time delay systems can provide a higher level of computational security against embedding reconstruction. (ii) TD systems provide hyperchaos with multiple positive Lyapunov exponents (LEs) [17]. Due to these reasons, a number of simple and well characterized TD systems have been designed to produce chaos and hyperchaos [18–20]. Dynamics of nonlinear time-delay systems have been studied [19, 21].

In this paper, we focus our attention towards the simple and well characterized first-order Ikeda TD system:

$$\dot{x}(t) = -ax(t) + b\sin(x_\tau), \tag{1}$$

where $a \in R$ and $b \in R$ are positive parameters, $\tau \in R^+$ is the time delay constant, and $x_\tau \equiv x(t-\tau)$. From the theoretical point of view, some works have been carried out with the aim of inherent dynamics of the Ikeda TD system. In [22], the chaotic dynamics of first-order scalar

delay differential equations, including Ikeda equations, have been investigated. An analytical framework for study of dynamics of breathers in slow-fast Ikeda optoelectronic systems was proposed in [23]. A study on the biorhythmic behavior and its control in an optoelectronic oscillator was presented in [24]. From the viewpoint of engineering, some research studies have focused on the performance enhancement of the system for random number generation, optical chaotic secure communication, chaotic image encryption, optical secret communication, and so on [25–31].

It is noted that chaotic dynamical properties such as high complexity and wide chaotic parameter range are strongly required in some scenarios, including secure communication and random number generation. But researchers found that existing chaotic systems have certain limitations in different aspects. One concern is that many systems suffered from the fragile chaos phenomenon [32]. Fragile chaos means that a system has small chaotic parameter regions or has some nonchaotic structures embedded in the chaotic parameter zone. Small perturbation modulation of a parameter of the system is possible to destroy the chaotic attractors and transform the chaotic oscillator to period oscillations, as the parameter will fall into a nonchaotic region easily. Moreover, due to the limitation of physical devices, the range of physical parameters is always restricted, which will cause performance degradation in many cases. A typical scenario is chaotic secure communication. The security level of a chaos-based scheme is significantly dependent on the chaotic parameter range [33].

Considering the fragile chaos phenomenon, this paper proposes an asymmetric central contraction mutation (ACCM) model to enhance the Ikeda TD system. The modified TD system with ACCM is studied. We carry out stability analysis to identify the parameter zone for which the system shows a stable equilibrium response. And we simulate the system model numerically to show that with the variation of delay and other system parameters, the system exhibits stable limit cycle, chaos, hyperchaos, and multiscroll hyperchaos over the whole three-dimensional (3D) parameter space (given by a, b, and τ). Single parameter bifurcation diagrams, phase plots, and two-parameter (2D) Lyapunov exponent diagrams [34] are employed to explore the dynamics of the system. The ACCM model not only can enhance the dynamical complexity of the original Ikeda TD system in the chaotic range, but also can produce chaos in the nonchaotic range. It is worth mentioning that the improved system has larger chaotic parameter zones with good connectivity.

The rest of the paper is arranged in the following order. Section 2 presents the related mathematical model of the proposed ACCM-Ikeda time delay system. Analysis of stability and Hopf bifurcation are shown in Section 3. Simulation results of the ACCM-Ikeda time delay system and discussions are presented in Section 4, followed by performance comparison in Section 5. Section 6 draws conclusion.

2. System Description

We propose the following Ikeda TD system with Asymmetric Central Contraction Mutation (ACCM):

$$\dot{x}(t) = -ax(t) + b\sin\left[x_\tau + \tanh\left(x_\tau\right) + \tanh\left(x_\tau - 2\right)\right], \tag{2}$$

where $a > 0$ and $b > 0$ are real positive system parameters. $x_\tau \equiv x(t-\tau)$, and $\tau \in R^+$ is the intrinsic time delay of the system.

Sketches of the nonlinearities $\sin(x_\tau)$, $\tanh(x_\tau)$, and $g(x_\tau) = \sin[x_\tau + \tanh(x_\tau) + \tanh(x_\tau - 2)]$ are depicted in Figures 1(a)–1(c), respectively. It can be found from Figure 1(c) that the sketch of nonlinearity $g(x_\tau)$ showing a variation law similar to that of the $\sin(x_\tau)$ function, but with asymmetric central contraction, emerging more humps and valleys in the curve within the same parameter range. Therefore, we named the modified model as the ACCM-Ikeda TD system, which will have expected dynamic characteristics, such as better complexity, more larger and connected (meaning that there is no transient nonchaotic window interspersed in the chaotic parameter zone) chaotic parameter zone than the seed Ikeda time delay system (will be discussed in Section 5).

3. Stability and Hopf Bifurcation Analysis

Consider the TD system (2) expressed as

$$\begin{aligned}\dot{x}(t) &= f\left(x, x_\tau\right)\\ &= -ax(t) + bg\left(x_\tau\right).\end{aligned} \tag{3}$$

Equilibrium points x^* of (3) are obtained by solving

$$f\left(x^*, x^*\right) = 0. \tag{4}$$

3.1. Linearization near Equilibrium. Defining a small perturbation $\delta = x - x^*$ in equilibrium solution and using first-order Taylor's approximation, we get a linearized equation of (3) as

$$\begin{aligned}\frac{\mathrm{d}\delta}{\mathrm{d}t} &= \frac{\mathrm{d}x}{\mathrm{d}t}\\ &= f\left(x, x_\tau\right)\\ &= f\left(x + \delta, x_\tau + \delta_\tau\right)\\ &= f\left(x^*, x^*\right) + \partial_1 f\left(x^*, x^*\right)\delta + \partial_2 f\left(x^*, x^*\right)\delta_\tau\\ &= p\delta + q\delta_\tau,\end{aligned} \tag{5}$$

where $x_\tau \equiv x(t-\tau)$, $\delta_\tau \equiv \delta(t-\tau)$, $p = \partial_1 f(x^*, x^*) = -a$, and $q = \partial_2 f(x^*, x^*) = bg'(x^*)$ are partial derivatives of $f(x, x_\tau)$ with respect to variables x and x_τ evaluated at (x^*, x^*), respectively. We can get the characteristic equation as

$$\lambda = -a + qe^{-\lambda\tau}. \tag{6}$$

3.2. Stability of Equilibrium. For the stability analysis, we use the methodology discussed in [22]. An equilibrium point x^*

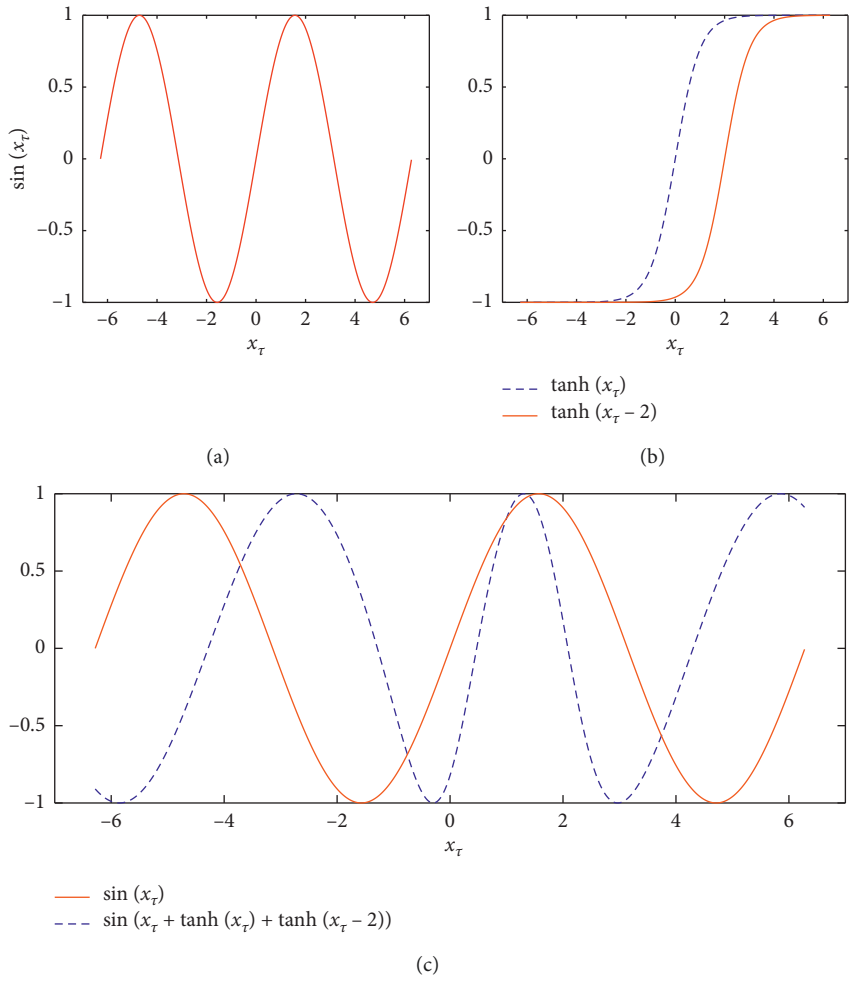

FIGURE 1: Sketches of (a) $\sin(x_\tau)$, (b) $\tanh(x_\tau)$ and $\tanh(x_\tau - 2)$, and (c) $g(x_\tau)$ (dotted line).

is asymptotically stable if all the roots λ_i of characteristic equation (6) satisfy

$$\mathrm{Re}(\lambda_i) < 0, \quad \text{for } \forall i. \tag{7}$$

If $\tau = 0$, then condition (7) takes the form

$$-a + q < 0. \tag{8}$$

Write $\lambda = u + i\omega$, $u, \omega \in R$. Stability of equilibrium will change if λ crosses imaginary axis at $\lambda = i\omega$. The characteristic equation in this case becomes

$$i\omega = -a + qe^{-i\omega\tau}. \tag{9}$$

Using $e^{-i\omega\tau} = \cos(\omega\tau) - i\sin(\omega\tau)$ and separating real and imaginary parts in (9), we get

$$\begin{cases} q\cos(\omega\tau) = a, \\ q\sin(\omega\tau) = -\omega. \end{cases} \tag{10}$$

This gives

$$q^2 = a^2 + \omega^2. \tag{11}$$

Then, we can get

$$\omega = \sqrt{q^2 - a^2}. \tag{12}$$

This is possible if and only if

$$|q| > a. \tag{13}$$

3.3. Critical Surfaces. For $|b| > a$, from (10) we can obtain the critical surfaces expressed as

$$\tau_k = \begin{cases} \dfrac{\cos^{-1}(a/bg'(x^*)) + 2k\pi}{\sqrt{q^2 - a^2}}, & \text{for } g'(x^*) < 0, \\ \dfrac{2\pi - \cos^{-1}(a/bg'(x^*)) + 2k\pi}{\sqrt{q^2 - a^2}}, & \text{for } g'(x^*) > 0. \end{cases} \tag{14}$$

Differentiating characteristic equation (6) with respect to τ, we get

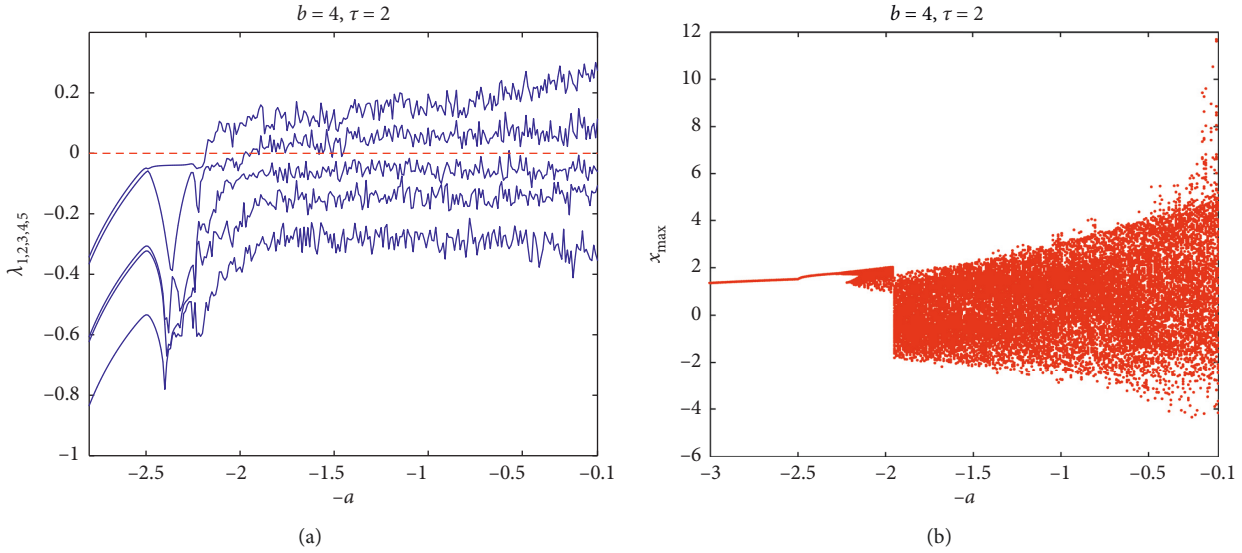

FIGURE 2: (a) The five largest Lyapunov exponents $\lambda_{1,2,3,4,5}$ plotted versus the bifurcation parameter $-3 \leq -a \leq -0.1$ for parameter $b = 4$ and time delay $\tau = 2$. (b) The bifurcation diagram for the same parameter as in case (a).

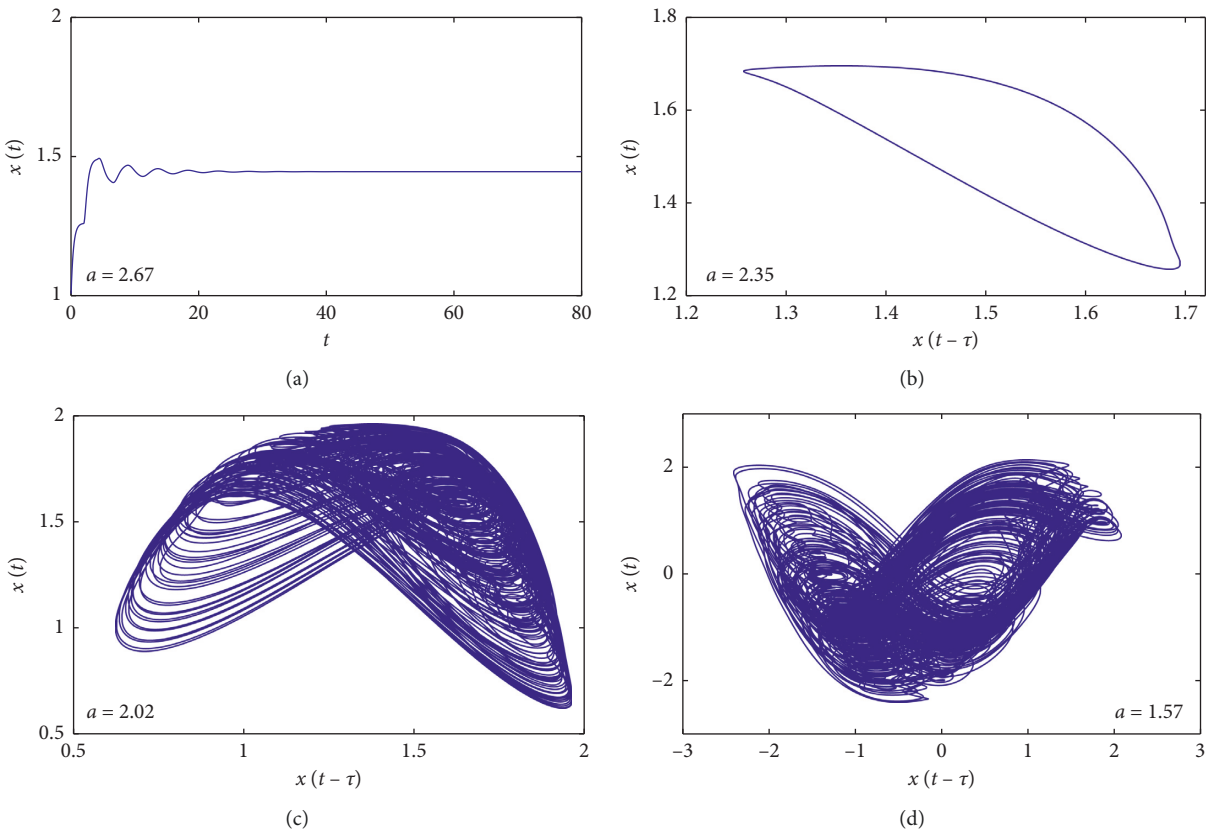

FIGURE 3: Continued.

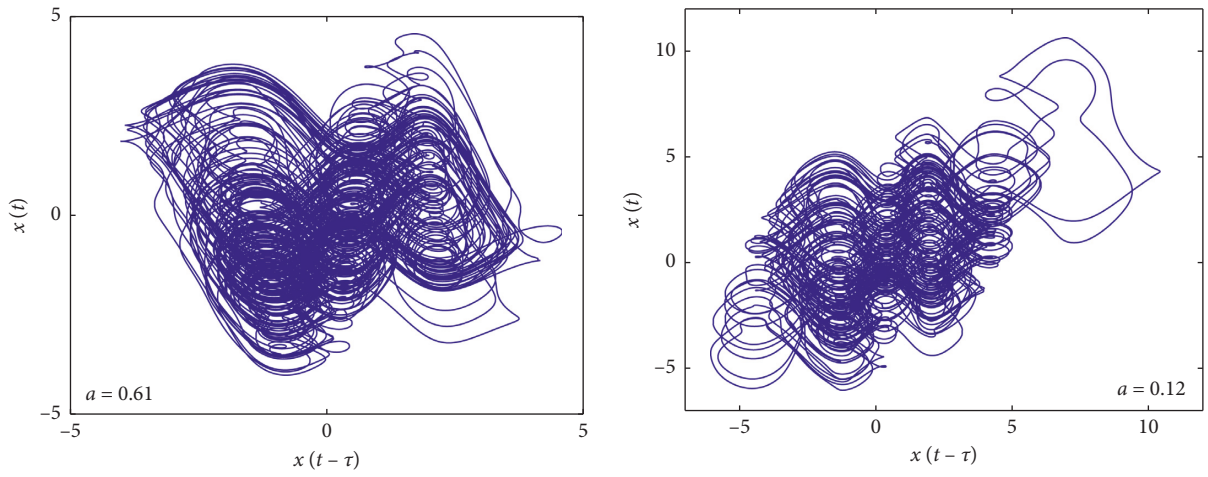

Figure 3: The initial condition is $\phi(t) = 1$ for $t \in [-\tau, 0]$ throughout the investigation. Parameter $b = 4$, and time delay $\tau = 2$. (a) Time series for $a = 2.67$, the fixed point is stable. Phase plane plots in $(x(t-\tau) - x(t))$ plane for variable a, (b) period limit cycle for $a = 2.35$, (c) chaotic attractor for $a = 2.02$, (d and e) hyperchaotic attractor for $a = 1.57$ and $a = 0.61$, (f) multiscroll hyperchaotic attractor for $a = 0.12$.

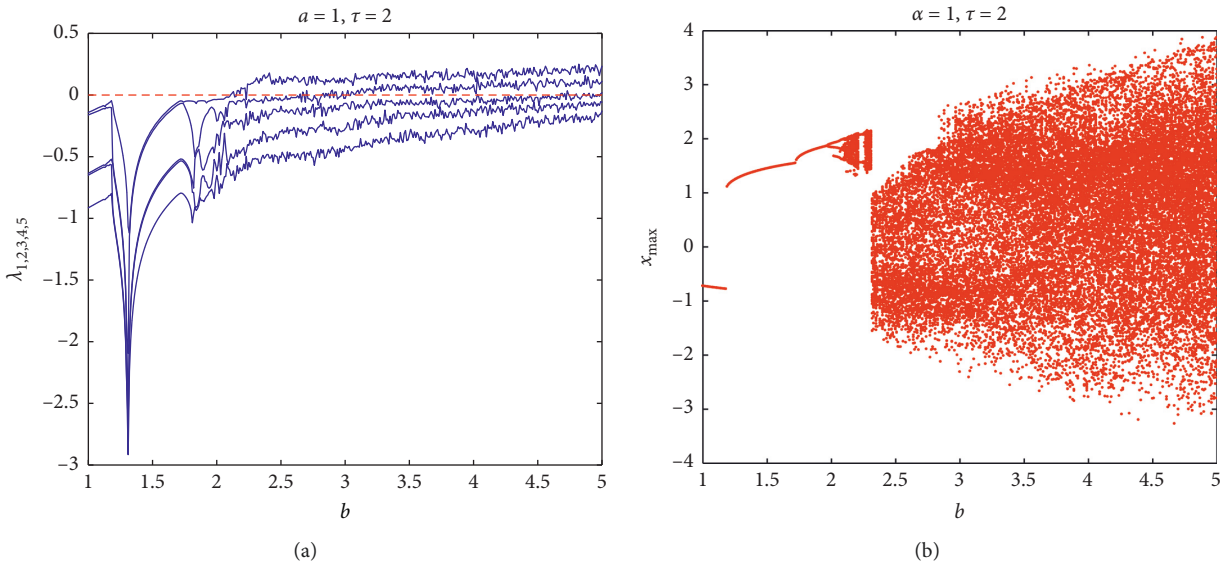

Figure 4: (a) The five largest Lyapunov exponents $\lambda_{1,2,3,4,5}$ plotted versus the bifurcation parameter $1 \le b \le 5$ for parameter $a = 1$ and time delay $\tau = 2$. (b) The bifurcation diagram for the same parameter as in case (a).

$$\frac{d\lambda}{d\tau} = qe^{-\lambda\tau}\left[-\lambda - \tau\frac{d\lambda}{d\tau}\right]. \tag{15}$$

Noting that $qe^{-\lambda\tau} = \lambda + a$, we can have

$$\frac{d\lambda}{d\tau} = -\frac{\lambda(\lambda + a)}{1 + \tau(\lambda + a)}, \tag{16}$$

and hence

$$\left.\frac{d\lambda}{d\tau}\right|_{u=0} = \frac{\omega^2 - ia\omega}{1 + a\tau + i\omega\tau}. \tag{17}$$

On critical surfaces (14),

$$\frac{d\lambda}{d\tau} = \mathrm{Re}\left(\frac{d\lambda}{d\tau}\right)\Big|_{u=0} = \frac{\omega^2}{(1 + a\tau)^2 + (\omega\tau)^2}, \tag{18}$$

$du/d\tau > 0$ on each of the critical surfaces τ_k. This implies that there does not exist any eigenvalue with negative real part across the critical surfaces (14). Thus, there is only one possible stability region (under condition (8)) enclosed by $\tau = 0$ and the critical surface τ_0 closest to it.

For $a > 0$, we have following main results:

Theorem 1. *Suppose x^* is an equilibrium solution of the ACCM-Ikeda TD system (3) and $q = \partial_2 f(x^*, x^*) = bg'(x^*)$, then we can get the following:*

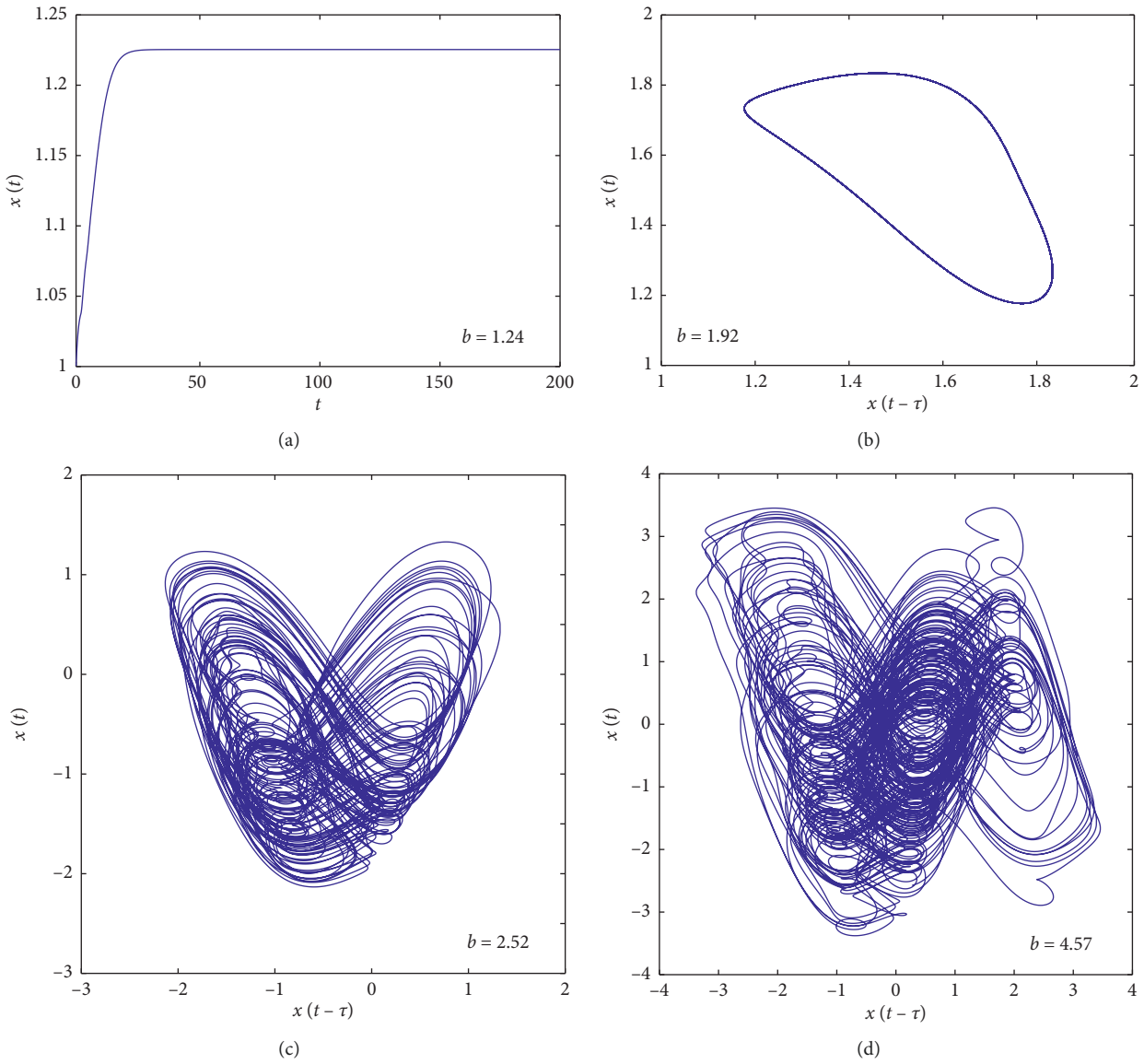

FIGURE 5: The initial condition is $\phi(t) = 1$ for $t \in [-\tau, 0]$ throughout the investigation. Parameter $a = 1$, and time delay $\tau = 2$. (a) Time series for $b = 1.24$, the fixed point is stable, (b) period limit cycles for $b = 1.92$, (c) chaotic attractors for $b = 2.52$, and (d) hyperchaotic attractors for $b = 4.57$.

(1) If $q \in (-\infty, -a)$, then the stability region of x^* in (τ, a, q) parameter space is located between the plane $\tau = 0$ and τ_0. ie equation undergoes Hopf bifurcation at this value.

(2) If $q \in (a, \infty)$, then x^* is unstable for any $\tau \geq 0$.

(3) If $q \in (-a, a)$, then x^* is stable for any $\tau \geq 0$.

4. Numerical Studies

In this section, the system equation (2) is solved numerically using the fourth-order Runge–Kutta algorithm with a step size $h = 0.01$. The initial condition is $\phi(t) = 1$ for $t \in [-\tau, 0]$ throughout the investigation. Then, the dynamics of the ACCM-Ikeda TD system is investigated through bifurcation diagram, phase plots, and Lyapunov exponent spectrum (LES) considered from different perspectives. The LES is calculated using the method proposed in [35].

4.1. Varying a for $b = 4$ and Time Delay $\tau = 2$. System (2) with parameter $b = 4$ and the time delay $\tau = 2$ is numerically examined for the single bifurcation parameter a. The bifurcation parameter a varies in the range $0.1 \leq a \leq 3$. Five largest Lyapunov exponents $\lambda_{1,2,3,4,5}$ of all the spectrum versus the bifurcation parameter a is shown in Figure 2(a), which reveals that,

(1) in the region $a \in [2.18, 3]$, the equilibrium point x^* is stable

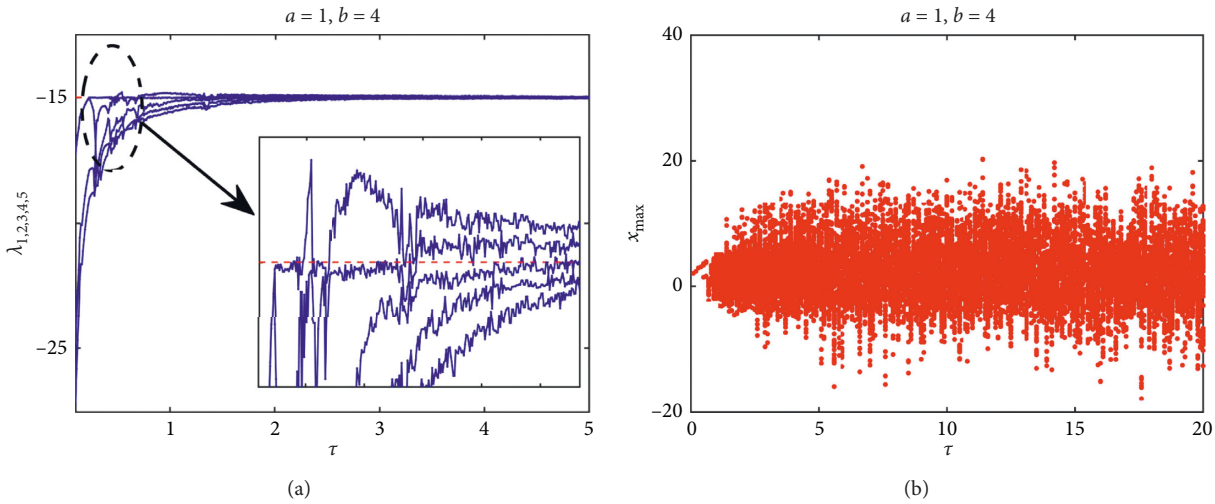

FIGURE 6: (a) The five largest Lyapunov exponents $\lambda_{1,2,3,4,5}$ plotted versus the time delay $0.1 \le \tau \le 20$ for parameters $a = 1$ and $b = 4$. (b) The bifurcation diagram for the same parameter as in case (a).

(2) in the region $a \in [1.9, 2.17]$, there is one positive LE ($\lambda_1 > 0$) meaning that chaos appears

(3) in the region $a \in [1.44, 1.89]$, chaotic and hyperchaotic regime appears alternately

(4) in the region a $\in [0.1, 1.43]$, there are two positive LE ($\lambda_1 > 0$ and $\lambda_2 > 0$) meaning that hyperchaos appears

These regions of nonchaos and chaos observed in Figure 2(a) are best visualized in the bifurcation diagram, where we plot the maxima of $x(t)$ versus the bifurcation parameter a, as shown in Figure 2(b). A good consistency can be noted between the bifurcation diagram and the LES. The outcomes of this variation are shown in Figure 3.

(i) For $a = 2.67$, we get equilibrium point $x^* = 1.44555$ and $q = bg'(x^*) = -2.0435$. By Case 3 of Theorem 1, the time series $x(t)$ converges to x^*, as shown in Figure 3(a).

(ii) For $a = 2.35$, we get equilibrium point $x^* = 1.53665$ and $q = bg'(x^*) = -3.4094$. Therefore, in view of Case 1 of Theorem 1, the stability region is located between $\tau = 0$ and $\tau_0 = 0.7564$. By setting $\tau = 2$, the equilibrium is found unstable leading to a limit cycle, as depicted in Figure 3(b).

(iii) For $a = 2.02$, we get $q = bg'(x^*) = -4.6290$. Therefore, in view of Case 1 of Theorem 1, the stability region is located between $\tau = 0$ and $\tau_0 = 0.4294$. By setting $\tau = 2$, the equilibrium is found unstable leading to a chaotic attractor, as depicted in Figure 3(c).

(iv) For $a = 1.57$, $a = 0.61$, and $a = 0.12$, we get $q = 7.5144$, $q = 7.8277$, and $q = 7.9023$. In view of Case 2 of Theorem 1, x^* is unstable for any $\tau \ge 0$. We can obtain hyperchaotic attractors (shown in Figures 3(d) and 3(e)) and a multiscroll hyperchaotic attractor (Figure 3(f)), respectively.

4.2. Varying b for a = 1 and Time Delay τ = 2. System (2) with the parameter $a = 1$ and the time delay $\tau = 2$ is numerically examined for the single bifurcation parameter b. The bifurcation parameter b varies in the range $1 \le b \le 5$. Five largest Lyapunov exponents $\lambda_{1,2,3,4,5}$ of all the spectrum versus the bifurcation parameter b is shown in Figure 4(a), which reveals that,

(1) in the region $1 \le b \le 2.1$, the equilibrium x^* is stable

(2) in the region $2.11 \le b \le 2.23$, chaotic and hyperchaotic regime appears alternately

(3) in the region $2.24 \le b \le 3$, there is one positive LE ($\lambda_1 > 0$) meaning that the chaos has appeared

(4) in the region $3.1 \le b \le 5$, there are two positive LE ($\lambda_1 > 0$ and $\lambda_2 > 0$) meaning that hyperchaos appears

These regions of nonchaos and chaos observed in Figure 4(a) are best visualized in the bifurcation diagram, where we plot the maxima of $x(t)$ versus the bifurcation parameter b, as shown in Figure 4(b). The outcomes of this variation are shown in Figure 5.

(i) For $b = 1.24$, we get $q = 0.3554$. x^* is stable in view of Case 3 of Theorem 1. And the solution converges to $x^* = 1.22535$, as shown in Figure 5(a).

(ii) For $b = 1.92$, we get $q = -2.1159$. In view of Case 1 of Theorem 1, the stability region is located between $\tau = 0$ and $\tau_0 = 1.1064$. By setting $\tau = 2$, the equilibrium is found unstable leading to a limit cycle, as depicted in Figure 5(b).

(iii) For $b = 2.52$ and $b = 4.57$, we get $q = 4.7286$ and $q = 8.8743$. By Case 2 of Theorem 1, we observe a chaotic attractor in Figure 5(c) and a hyperchaotic attractor in Figure 5(d), respectively.

4.3. Varying Time Delay τ for a = 1 and b = 4. System (2) with the parameter $a = 1$ and $b = 4$ is numerically examined for

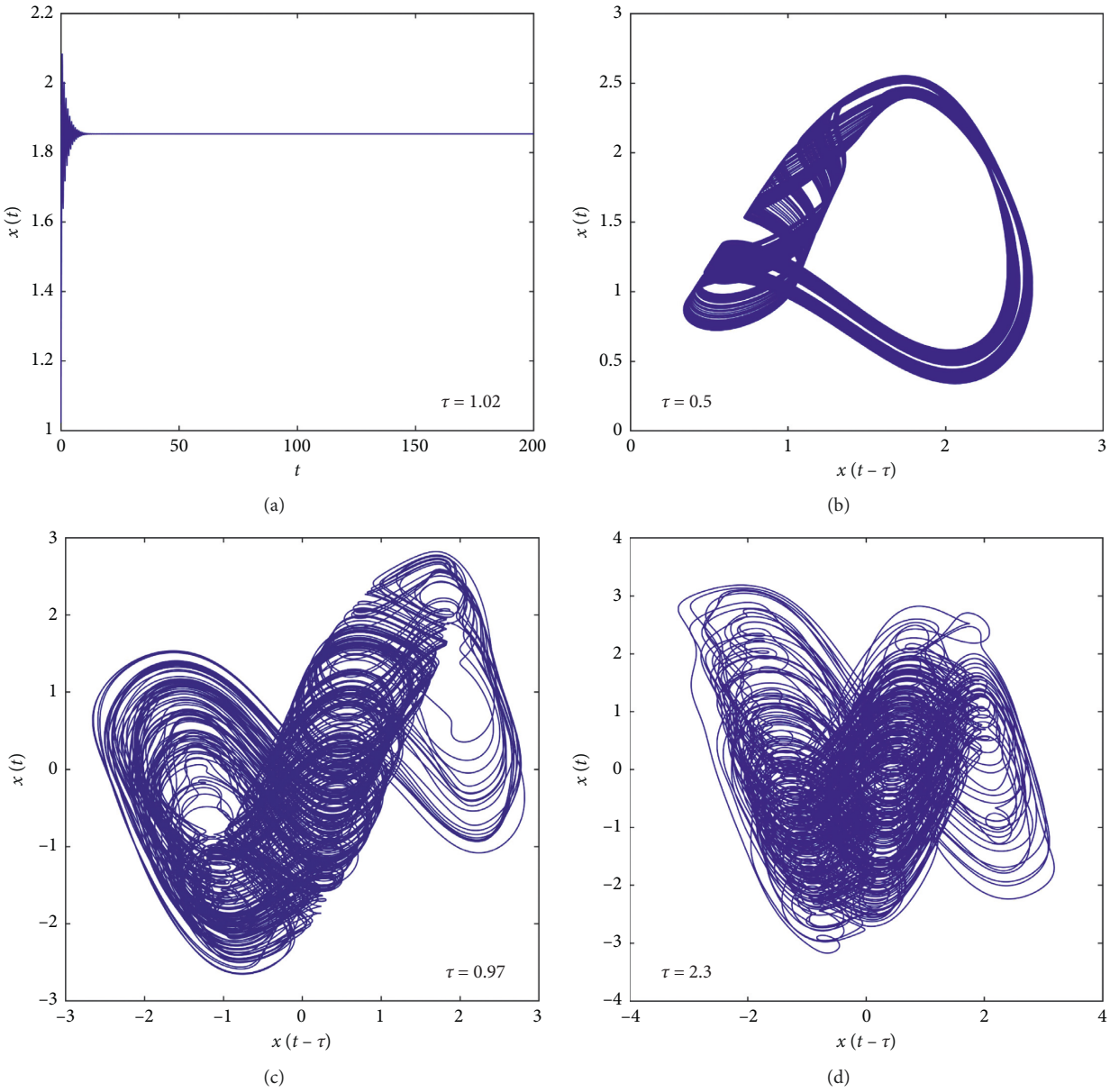

FIGURE 7: The initial condition is $\phi(t) = 1$ for $t \in [-\tau, 0]$ throughout the investigation. Parameters $a = 1$ and $b = 4$. (a) Period limit cycle for $\tau = 0.2$, (b and c) chaos attractors for $\tau = 0.5$ and $\tau = 0.97$, and (d) multiscroll hyperchaotic attractors for $\tau = 2.3$.

the time delay τ. The time delay τ varies in the range $0.1 \le \tau \le 20$. Five largest Lyapunov exponents $\lambda_{1,2,3,4,5}$ of all the spectrum versus the time delay τ is shown in Figure 6(a), which reveals that there is a narrow region of chaos ($\lambda_1 > 0$) between $0.48 \le \tau \le 0.54$ and $0.7 \le \tau \le 1.33$. When τ is starting at about 1.45, there is already a permanent hyperchaos (λ_1, $\lambda_2 > 0$) range.

These regions of nonchaos and chaos observed in Figure 6(a) are best visualized in the bifurcation diagram, where we plot the maxima of $x(t)$ versus the time delay τ, as shown in Figure 6(b).

For $a = 1$ and $b = 4$, we get $x^* = 1.853$ and $q = bg'(x^*) = -7.3430$, then x^* is stable in view of Case 1 of Theorem 1 and the stability region is located between $0 \le \tau \le 0.2347$. The outcomes of this variation are shown in Figure 7.

(i) For $\tau = 0.2 < \tau_0$, x^* is stable and the solution converges to $x^* = 1.853$, as shown in Figure 7(a)

(ii) Chaos attractors for $\tau = 0.5$ and $\tau = 0.97$ are shown in Figures 7(b) and 7(c)

(iii) At $\tau = 2.3$ a hyperchaotic attractor is exhibited in Figure 7(d)

5. Performance Evaluations

To exhibit the effect of the ACCM in enhancing the chaotic dynamic characteristics of the Ikeda TD system, we compare the chaos and hyperchaos characteristics of the improved system with that of the seed Ikeda TD system. The systems are integrated with a fourth-order Runge–Kutta algorithm,

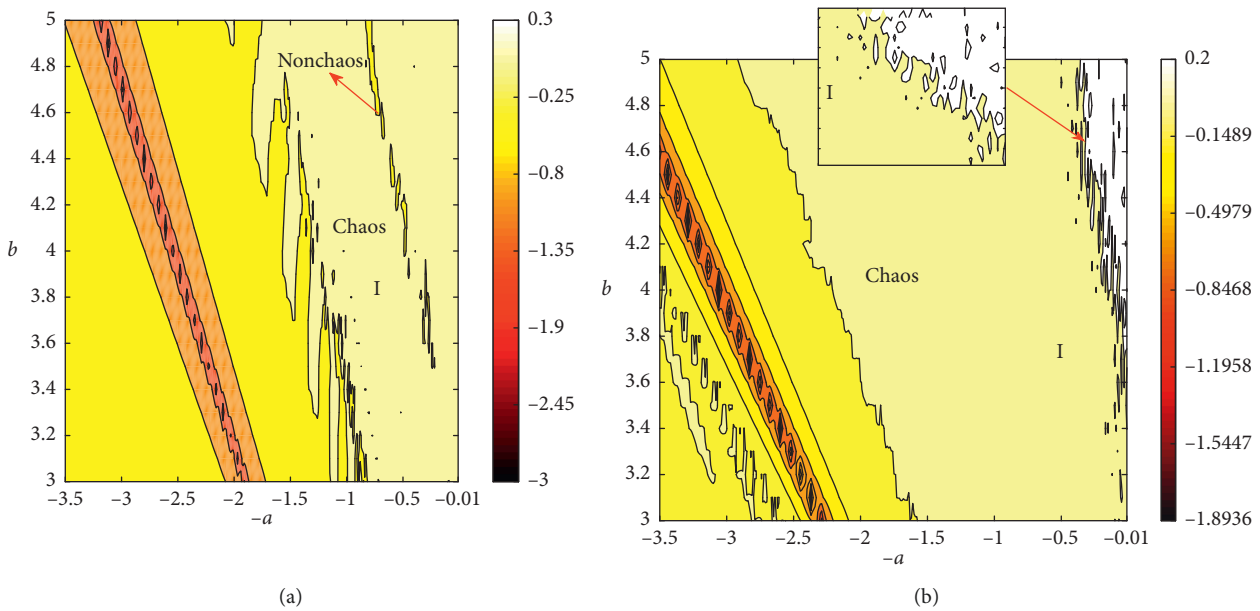

(a) (b)

Figure 8: (a) The 2D LE diagram showing the largest Lyapunov exponent (λ_1) of the Ikeda TD system in the ($a - b$) space. (b) The 2D LE diagram showing the largest Lyapunov exponent of the ACCM-Ikeda TD system in the ($a - b$) space.

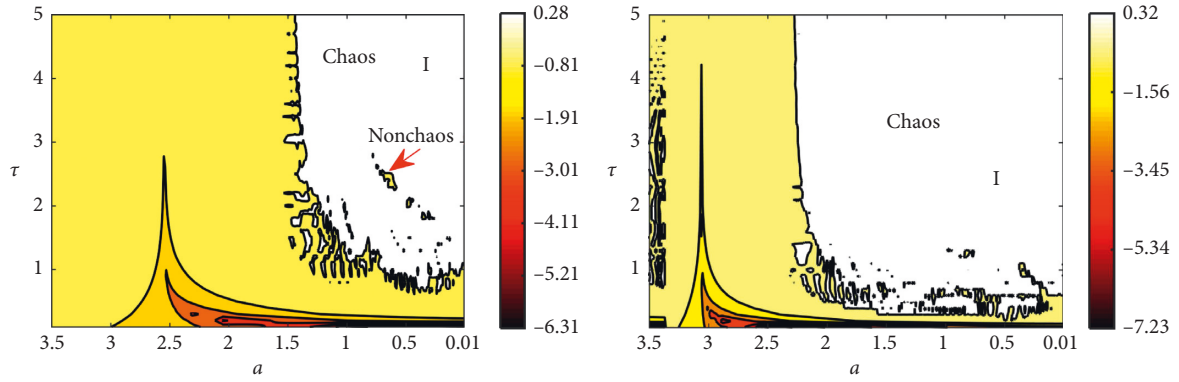

(a) (b)

Figure 9: (a) The 2D LE diagram showing the largest Lyapunov exponent (λ_1) of the Ikeda TD system in the ($a - \tau$) space. (b) The 2D LE diagram showing the largest Lyapunov exponent of the ACCM-Ikeda TD system in the ($a - \tau$) space.

with a fixed time step size equal to $h = 0.01$. Two-parameter (2D) Lyapunov exponent diagrams are employed to explore the dynamics of the systems over the whole three-dimensional (3D) parameter space (given by a, b, and τ).

5.1. 2D Largest Lyapunov Exponent Diagrams. The chaotic dynamical behaviors of the ACCM-Ikeda and seed Ikeda TD systems over the whole (a, b), (a, τ), and (b, τ) parameter space are presented in this section. All of these 2D parameter space diagrams are obtained by considering the LLE value. The results for a cut of this 3D space at $\tau = 2$, $b = 4$, and $a = 1$ are shown in Figures 8–10. The white and faint yellow zones (noted by I) indicate the chaotic dynamics of the system ($\lambda_1 > 0$). In Figure 8(a), some stripes corresponding to nonchaotic regions embedded in the chaos region can be found. In Figure 8(b), we can find a larger connected chaos region. The ACCM-Ikeda TD system has larger connected chaos region in the (a, b) space. And from Figures 9 and 10, we can get the same results. The ACCM-Ikeda TD system has larger connected chaos region over the whole (a, b), (a, τ), and (b, τ) parameter space. Moreover, it is noteworthy that with increasing b smaller time delay of the ACCM-Ikeda TD system is required to produce chaos (Figure 10(b)).

5.2. 2D Second Largest Lyapunov Exponent. The hyperchaotic dynamical behaviors of the ACCM-Ikeda and seed Ikeda TD systems over the whole (a, b), (a, τ), and (b, τ) parameter space are presented in this section. Hyperchaotic dynamical behavior is studied by using the second largest

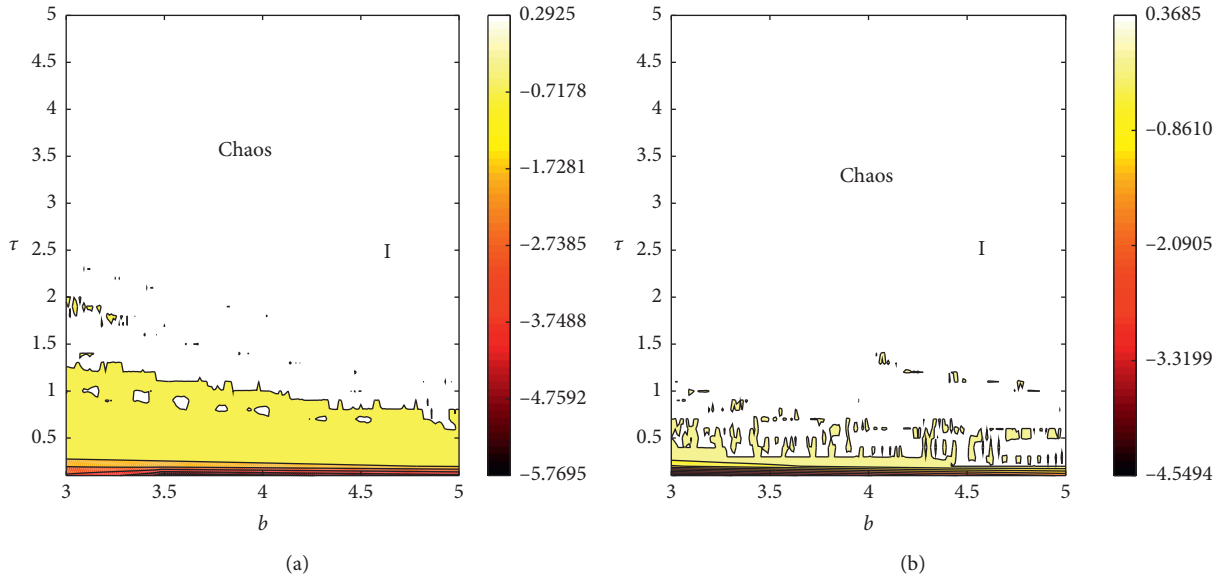

Figure 10: (a) The 2D LE diagram showing the largest Lyapunov exponent (λ_1) of the Ikeda TD system in the $(b - \tau)$ space. (b) The 2D LE diagram showing the largest Lyapunov exponent of the ACCM-Ikeda TD system in the $(b - \tau)$ space.

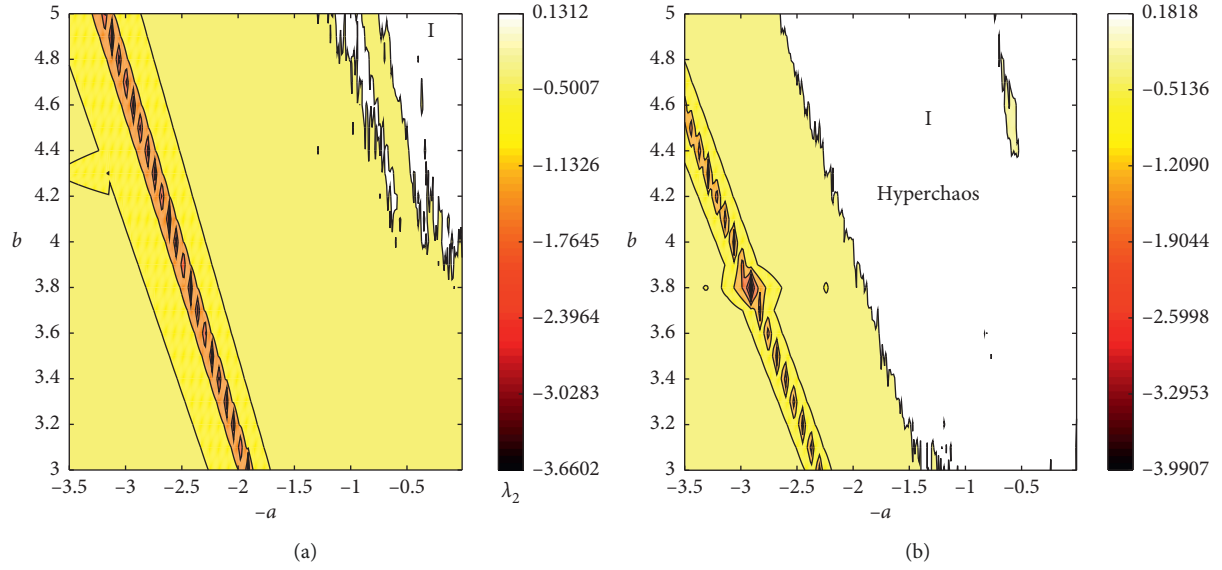

Figure 11: (a) The 2D LE diagram showing the second largest Lyapunov exponent (λ_2) of the Ikeda TD system in the $(a - b)$ space. (b) The 2D LE diagram showing the second largest Lyapunov exponent of the ACCM-Ikeda TD system in the $(a - b)$ space.

Lyapunov exponent (LE_2) as indicators. As shown in Figures 11–13, the white and faint yellow zones (noted by I) indicate the hyperchaotic states of the system ($\lambda_2 > 0$ and $\lambda_1 > 0$, in Figures 8–10). Clearly in Figures 11–13, the ACCM-Ikeda TD system has larger connected hyperchaotic regions in 2D parameter spaces (a, b), (a, τ), and (b, τ). With parameters $-a$, b, and time delay τ increase, λ_2 of the enhanced ACCM-Ikeda TD system become larger and positive when λ_2 of the original Ikeda system is still negative. As such, the ACCM model can transform the chaotic oscillator to hyperchaotic oscillations.

5.3. Largest Lyapunov Exponent. Moreover, the complexity of the two systems is compared by calculating the single parameter Largest Lyapunov Exponent. Lyapunov Exponent can describe the average separation rate of trajectories starting from two extremely close initial states. A positive LE means that the two adjacent trajectories of a dynamical system exponentially separate in each iteration. A dynamical system with a positive LE is regarded as chaotic, and larger LE represents higher dynamical complexity. Figures 14(a)–14(c) compare the largest Lyapunov exponents (LLEs) of the ACCM-Ikeda TD system and its associated seed Ikeda

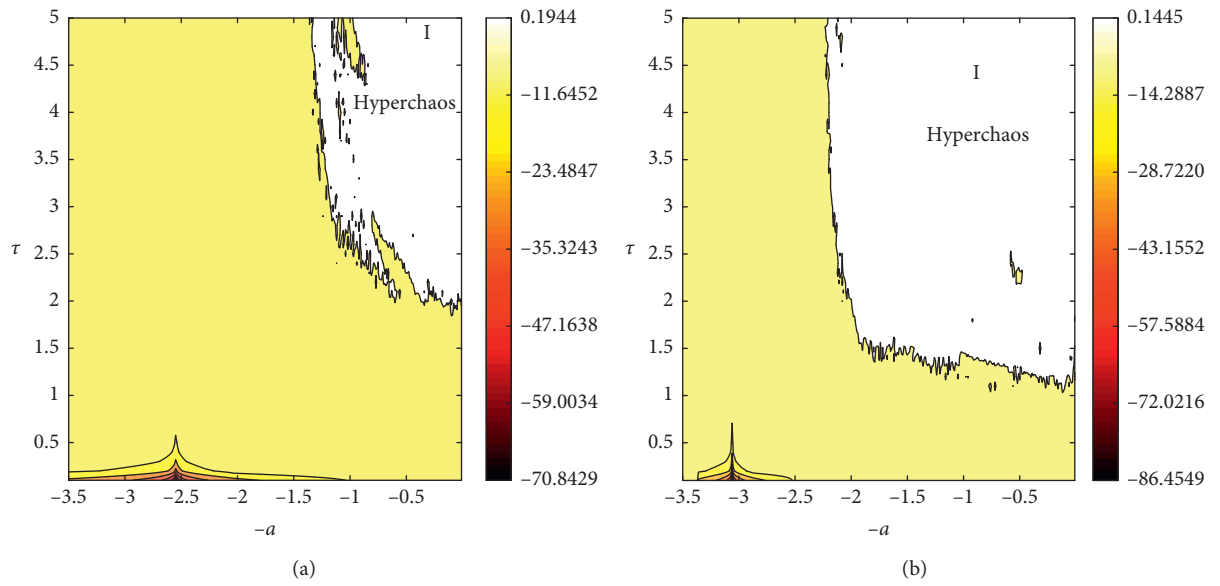

Figure 12: (a) The 2D LE diagram showing the second largest Lyapunov exponent (λ_2) of the Ikeda TD system in the $(a - \tau)$ space. (b) The 2D LE diagram showing the second largest Lyapunov exponent of the ACCM-Ikeda TD system in the $(a - \tau)$ space.

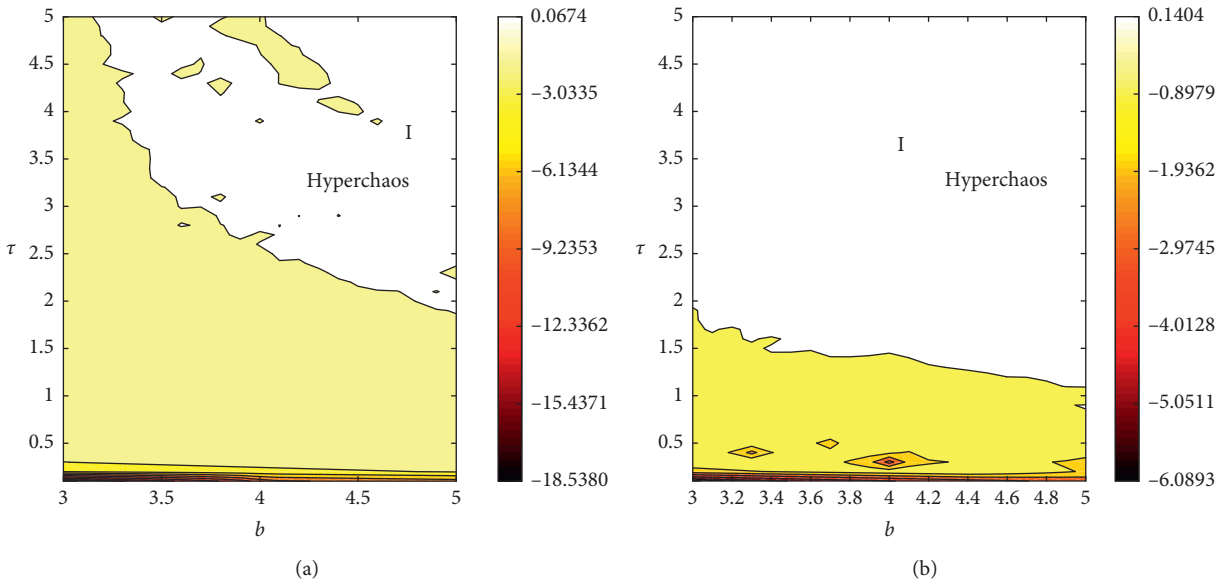

Figure 13: (a) The 2D LE diagram showing the second largest Lyapunov exponent (λ_2) of the Ikeda TD system in the $(b - \tau)$ space. (b) The 2D LE diagram showing the second largest Lyapunov exponent of the ACCM-Ikeda TD system in the $(b - \tau)$ space.

system. The largest Lyapunov exponents (LLEs) curve with the change of parameters a, b, and time delay τ, as shown in Figures 11(a) and 11(b), respectively. As can be observed from these figures that the ACCM-Ikeda TD system has larger LLEs, it proves that ACCM can enhance the chaos complexity of the original Ikeda system.

6. Conclusion

In this paper, a new Ikeda time delay system with asymmetric central contraction mutation (ACCM) is proposed and examined. First, we have analyzed the stability and Hopf bifurcation of the system. The results for different types of stability regions are derived. The conditions on the partial derivatives of function f at equilibrium points are provided theoretically. The Hopf bifurcation value of delay τ is also mentioned. Next, the dynamical analysis of the system is carried out by visualizing the bifurcation diagram and spectrum of the first five LEs as a function of system parameters a, b, and the time delay τ. In a large range of parameters, rich dynamical behaviors including asymptotic stability, limit cycles, chaos, hyperchaos, and multiscroll chaos are observed. Finally, we have compared the chaotic dynamics of the ACCM-Ikeda TD system and those of the

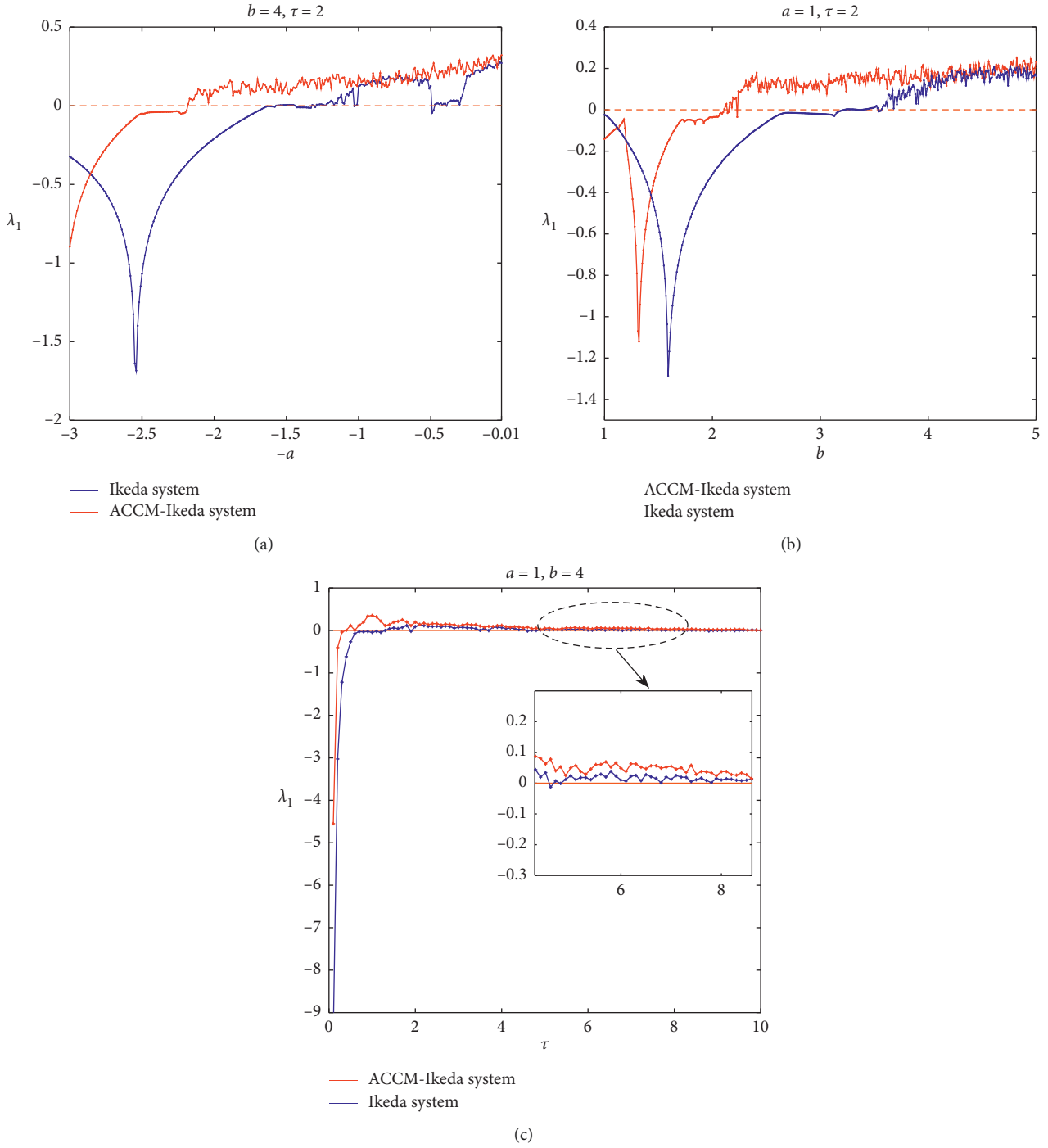

FIGURE 14: The first largest LEs comparisons of the ACCM-Ikeda TD system (2) and the seed Ikeda TD system (1): (a) LLE (λ_1) comparison for bifurcation parameter a; (b) LLE (λ_1) comparison for bifurcation parameter b; (c) LLE (λ_1) comparison for bifurcation parameter τ.

seed Ikeda TD system. Two-parameter (2D) LE diagrams are employed to explore the chaotic dynamics of the system over the whole parameter space. Complexity of the systems is characterized by LLE as a function of single parameter. The simulation results show that the ACCM-Ikeda TD system has higher complexity and larger chaotic and hyperchaotic parameter zones. There is no transient nonchaos window, and the fragile chaos phenomenon is successfully suppressed. Moreover, chaotic regime can be transformed to hyperchaotic regime by introducing the ACCM strategy. As a theoretical extension of the Ikeda TD system, the proposed scheme could be realized by the combination of electrical and optical devices according to some existing research studies [28, 36], and the ACCM-Ikeda TD system has the potential to be used in real world applications such as secure communications and random number generation.

Data Availability

The data used to support the findings of this study are available from the corresponding author upon request.

Conflicts of Interest

The author declares that there are no conflicts of interest.

References

[1] J. Chen, F. Min, Q. Jin, and B. Ye, "Coexistence, bifurcation and chaos of a periodically forced duffing system with absolute nonlinearity," *The European Physical Journal Special Topics*, vol. 228, no. 6, pp. 1405–1419, 2019.

[2] M. Inubushi, "Unpredictability and robustness of chaotic dynamics for physical random number generation," *Chaos: An Interdisciplinary Journal of Nonlinear Science*, vol. 29, no. 3, Article ID 033133, 2019.

[3] H. Wang and G. Dong, "New dynamics coined in a 4-d quadratic autonomous hyper-chaotic system," *Applied Mathematics and Computation*, vol. 346, pp. 272–286, 2019.

[4] H. Liu, Y. Zhang, A. Kadir, and Y. Xu, "Image encryption using complex hyper chaotic system by injecting impulse into parameters," *Applied Mathematics and Computation*, vol. 360, pp. 83–93, 2019.

[5] L. Wang, T. Dong, and M.-F. Ge, "Finite-time synchronization of memristor chaotic systems and its application in image encryption," *Applied Mathematics and Computation*, vol. 347, pp. 293–305, 2019.

[6] S. Vaidyanathan, A. Akgul, S. Kaçar, and U. Çavuşoğlu, "A new 4-d chaotic hyperjerk system, its synchronization, circuit design and applications in RNG, image encryption and chaos-based steganography," *The European Physical Journal Plus*, vol. 133, no. 2, p. 46, 2018.

[7] M. Li, Y. Hong, Y. Song, and X. Zhang, "Effect of controllable parameter synchronization on the ensemble average bit error rate of space-to-ground downlink chaos laser communication system," *Optics Express*, vol. 26, no. 3, pp. 2954–2964, 2018.

[8] L. Liu and S. Miao, "An image encryption algorithm based on baker map with varying parameter," *Multimedia Tools & Applications*, vol. 76, no. 15, pp. 16511–16527, 2017.

[9] H. Hu, L. Liu, Y. Deng, and S. Miao, "Pseudorandom bit generator based on non-stationary logistic maps," *IET Information Security*, vol. 10, no. 2, pp. 87–94, 2016.

[10] Ü. Çavuşoğlu, S. Kaçar, A. Zengin, and I. Pehlivan, "A novel hybrid encryption algorithm based on chaos and S-AES algorithm," *Nonlinear Dynamics*, vol. 92, no. 4, pp. 1745–1759, 2018.

[11] D. M. Wang, L. S. Wang, Y. Y. Guo, Y. C. Wang, and A. B. Wang, "Key space enhancement of optical chaos secure communication: chirped FBG feedback semiconductor laser," *Optics Express*, vol. 27, no. 3, pp. 3065–3073, 2019.

[12] H. Yin, Q. Zhao, D. Xu et al., "1.25 Gbits/s-message experimental transmission utilising chaos-based fibre-optic secure communications over 143 km," *International Journal of High Performance Computing and Networking*, vol. 14, no. 1, pp. 42–51, 2019.

[13] L. Wang, Y. Guo, D. Wang, Y. Wang, and A. Wang, "Experiment on 10-Gb/s message transmission using an all-optical chaotic secure communication system," *Optics Communications*, vol. 453, Article ID 124350, 2019.

[14] S. Ergun, "Vulnerability analysis of a chaos-based random number generator," in *Proceedings of the 2018 IEEE International Conference on Systems, Man, and Cybernetics (SMC)*, pp. 3331–3334, IEEE, Miyazaki, Japan, February 2018.

[15] H. Natiq, M. R. K. Ariffin, M. R. M. Said, and S. Banerjee, "Enhancing the sensitivity of a chaos sensor for internet of things," *Internet of Things*, vol. 7, Article ID 100083, 2019.

[16] T. Banerjee, D. Biswas, and B. C. Sarkar, "Design and analysis of a first order time-delayed chaotic system," *Nonlinear Dynamics*, vol. 70, no. 1, pp. 721–734, 2012.

[17] H. Wernecke, B. Sándor, and C. Gros, "Chaos in time delay systems, an educational review," *Physics Reports*, vol. 824, pp. 1–40, 2019.

[18] D. V. Senthilkumar, K. Srinivasan, K. Murali, M. Lakshmanan, and J. Kurths, "Experimental confirmation of chaotic phase synchronization in coupled time-delayed electronic circuits," *Physical Review E*, vol. 82, Article ID 065201, 2010.

[19] K. Srinivasan, I. Raja Mohamed, K. Murali, M. Lakshmanan, and S. Sinha, "Design of time delayed chaotic circuit with threshold controller," *International Journal of Bifurcation and Chaos*, vol. 21, no. 3, pp. 725–735, 2011.

[20] D. Biswas and T. Banerjee, "Chaotic time-delayed system with hard nonlinearity: design and characterization," in *Time-Delayed Chaotic Dynamical Systems*, Springer, Berlin, Germany, 2018.

[21] M. Lakshmanan and D. V. Senthilkumar, *Dynamics of Nonlinear Time-Delay Systems*, Springer Science & Business Media, Berlin, Germany, 2011.

[22] J. Wei, "Bifurcation analysis in a scalar delay differential equation," *Nonlinearity*, vol. 20, no. 11, pp. 2483–2498, 2007.

[23] J. H. T. Mbé, A. F. Talla, G. R. G. Chengui et al., "Mixed-mode oscillations in slow-fast delayed optoelectronic systems," *Physical Review E*, vol. 91, no. 1, Article ID 012902, 2015.

[24] D. Ghosh, A. Mukherjee, N. R. Das, and B. Biswas, "Control of coexisting periodic oscillations in an optoelectronic oscillator," *Optical Engineering*, vol. 57, no. 12, Article ID 126108, 2018.

[25] M. Li, H. Fan, Y. Xiang, Y. Li, and Y. Zhang, "Cryptanalysis and improvement of a chaotic image encryption by first-order time-delay system," *IEEE MultiMedia*, vol. 25, no. 3, pp. 92–101, 2018.

[26] W. Shao, M. Cheng, C. Luo et al., "An image encryption scheme based on hybrid electro-optic chaotic sources and compressive sensing," *IEEE Access*, vol. 7, pp. 156582–156591, 2019.

[27] Z. Zhao, M. Cheng, C. Luo et al., "Semiconductor-laser-based hybrid chaos source and its application in secure key distribution," *Optics Letters*, vol. 44, no. 10, pp. 2605–2608, 2019.

[28] Y. Fu, M. Cheng, X. Jiang et al., "High-speed optical secure communication with an external noise source and an internal time-delayed feedback loop," *Photonics Research*, vol. 7, no. 11, pp. 1306–1313, 2019.

[29] Z. Zhao, M. Cheng, C. Luo et al., "Synchronized random bit sequences generation based on analog-digital hybrid electro-optic chaotic sources," *Journal of Lightwave Technology*, vol. 36, no. 20, pp. 4995–5002, 2018.

[30] R. M. Nguimdo, P. Colet, L. Larger, and L. Pesquera, "Digital key for chaos communication performing time delay concealment," *Physical Review Letters*, vol. 107, no. 3, Article ID 034103, 2011.

[31] S. Miao and L. Liu, "Two-dimensional electro-optic delayed feedback system with electrical and optical coupling," *IET Optoelectronics*, vol. 12, no. 3, pp. 156–160, 2018.

[32] Z. Hua, B. Zhou, and Y. Zhou, "Sine chaotification model for enhancing chaos and its hardware implementation," *IEEE*

Transactions on Industrial Electronics, vol. 66, no. 2, pp. 1273–1284, 2019.

[33] X. Gao, F. Xie, and H. Hu, "Enhancing the security of electro-optic delayed chaotic system with intermittent time-delay modulation and digital chaos," *Optics Communications*, vol. 352, pp. 77–83, 2015.

[34] T. F. Fozin, P. M. Ezhilarasu, Z. N. Tabekoueng et al., "On the dynamics of a simplified canonical chua's oscillator with smooth hyperbolic sine nonlinearity: hyperchaos, multi-stability and multistability control," *Chaos: An Interdisciplinary Journal of Nonlinear Science*, vol. 29, no. 11, Article ID 113105, 2019.

[35] J. D. Farmer, "Chaotic attractors of an infinite-dimensional dynamical system," *Physica D Nonlinear Phenomena*, vol. 4, no. 3, pp. 366–393, 1982.

[36] D. Biswas, B. Karmakar, and T. Banerjee, "A hyperchaotic time-delayed system with single-humped nonlinearity: theory and experiment," *Nonlinear Dynamics*, vol. 89, no. 58, pp. 1733–1743, 2017.